A General Linear Relaxometry Model of R_1 Using Imaging Data

Martina F. Callaghan,[1]* Gunther Helms,[2] Antoine Lutti,[3] Siawoosh Mohammadi,[1] and Nikolaus Weiskopf[1]

Purpose: The longitudinal relaxation rate (R_1) measured in vivo depends on the local microstructural properties of the tissue, such as macromolecular, iron, and water content. Here, we use whole brain multiparametric in vivo data and a general linear relaxometry model to describe the dependence of R_1 on these components. We explore a) the validity of having a single fixed set of model coefficients for the whole brain and b) the stability of the model coefficients in a large cohort.
Methods: Maps of magnetization transfer (MT) and effective transverse relaxation rate (R_2^*) were used as surrogates for macromolecular and iron content, respectively. Spatial variations in these parameters reflected variations in underlying tissue microstructure. A linear model was applied to the whole brain, including gray/white matter and deep brain structures, to determine the global model coefficients. Synthetic R_1 values were then calculated using these coefficients and compared with the measured R_1 maps.
Results: The model's validity was demonstrated by correspondence between the synthetic and measured R_1 values and by high stability of the model coefficients across a large cohort.
Conclusion: A single set of global coefficients can be used to relate R_1, MT, and R_2^* across the whole brain. Our population study demonstrates the robustness and stability of the model. **Magn Reson Med 73:1309–1314, 2015. © 2014 The Authors. Magnetic Resonance in Medicine published by Wiley Periodicals, Inc. This is an open access article under the terms of the Creative Commons Attribution License, which permits use, distribution and reproduction in any medium, provided the original work is properly cited.**

Key words: R_1; T_1; PD; PD*; MT; R_2^*; T_2^*; longitudinal relaxation; transverse relaxation; magnetization transfer; quantitative; 3T; water content; relaxometry

[1]Wellcome Trust Centre for Neuroimaging, Institute of Neurology, University College London, London, United Kingdom.

[2]MR Research in Neurology and Psychiatry, Department of Cognitive Neurology, University Medical Center, Goettingen, Germany.

[3]LREN, Department des Neurosciences Cliniques, CHUV, Universite de Lausanne, Lausanne, Switzerland.

*Correspondence to: Martina F. Callaghan, Wellcome Trust Centre for Neuroimaging, UCL Institute of Neurology, University College London, London, WC1N 3BG, UK. E-mail: m.callaghan@ucl.ac.uk.

INTRODUCTION

At a given field strength, the rate of longitudinal recovery ($R_1 = 1/T_1$) is determined by the microstructural tissue environment (eg, the local mobility of water molecules), the macromolecular content, and the local concentration of paramagnetic ions such as iron or gadolinium-based contrast agents. The linear dependence of R_1 on these tissue properties has been modeled and verified with independent laboratory measures from excised tissue (1–7) or by reference to literature values in the case of iron content (8).

Rapid cross-relaxation with macromolecules facilitates energy exchange between excited protons and their local environment, increasing the observed R_1 recovery rate. When macromolecular protons are selectively saturated using off-resonance radiofrequency (RF) irradiation, the MR water signal is attenuated by magnetization transfer (MT) (9). In MRI of humans, MT contrast is invoked by application of off-resonant RF pulses prior to excitation. In voxels with a higher macromolecular content, the mobile water will experience a greater percentage loss of signal (MT saturation) (10) as a consequence of a given prepulse and the dynamic of the MT (11). Consequently, measures of MT provide information about the macromolecular content of the microstructural environment and provide us with surrogate markers or model estimates for the bound water fraction (12). In a gradient echo acquisition, the observed MR signal created after RF excitation decays over time by the effective transverse relaxation rate ($R_2^* = 1/T_2^*$). The presence of paramagnetic metals, including iron, leads to local distortion of the static B_0 field causing a more rapid decay (ie, higher R_2^*) (13).

In this study, we used a quantitative multiparameter mapping (MPM) protocol to acquire whole brain quantitative maps of the longitudinal relaxation rate (R_1), effective transverse relaxation rate (R_2^*), and percent saturation due to MT. We used a linear model of R_1 that is motivated by the linear dependence of the measured R_1 on the relaxation rates of the individual spin pools under the conditions of fast exchange between pools. The measured MT saturation and R_2^* estimates served as surrogate concentrations for macromolecules and iron, respectively, to calculate the model coefficients. The validity of estimating a single set of model coefficients for the whole brain—including gray matter, white matter, and deep gray matter structures—was assessed by calculating the Pearson coefficient between the measured R_1 values and synthetic R_1 values generated using the model coefficients. A set of model coefficients was calculated individually for each of 138 volunteers to examine their stability across a population.
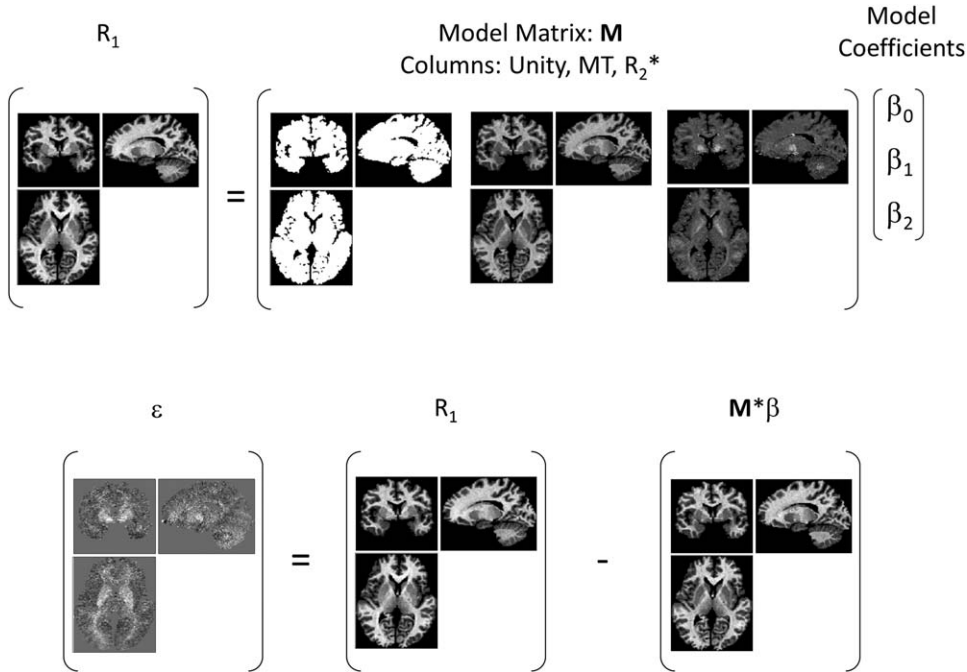
FIG. 1. Illustration of the linear relaxometry model that is constructed on a per-subject basis. The three model coefficients are the least squares solution to the matrix equation $R_1 = \mathbf{M}\beta$.

METHODS

Data Acquisition

A whole brain quantitative MPM protocol (14) was used to acquire 1-mm isotropic data from 138 healthy volunteers (male, n = 49; female, n = 89; age range, 19–75 y [mean age, 46.6 y; standard deviation, 21 y]) on two 3T whole body MR systems (Magnetom TIM Trio, Siemens Healthcare, Erlangen, Germany, 69 volunteers per scanner) each equipped with a standard 32-channel head coil for receive and RF body coil for transmission. The protocol consisted of PD-, T_1-, and MT-weighted multiecho FLASH acquisitions and additional B_1 field calibrations as described by Weiskopf et al. (14). The total scanning time of the MPM protocol was ~25 min. Informed written consent was obtained prior to scanning with approval from the local ethics committee.

Quantitative maps were derived from the MPM protocol using bespoke MATLAB tools (Mathworks, Natick, Massachusetts, USA). In brief, regression of the log signal from the eight PD-weighted echoes was used to calculate a map of R_2^*. The first six echoes of each of the three acquired weightings were then averaged to increase the signal-to-noise ratio (15). The resulting PD-weighted, T1-weighted, and MT-weighted volumes were used to calculate maps of MT and R_1 as described previously (10,14,16). To maximize the accuracy of the R_1 maps, inhomogeneity in the flip angle was corrected by mapping the B_1^+ transmit field according to the procedure detailed in the study by Lutti et al. (17) and the intrinsically imperfect spoiling characteristics were corrected using the approach described by Preibisch and Deichmann (18). Use of the measured R_1 maps in in vivo histological studies illustrated the high level of accuracy of the technique (19–21).

The semiquantitative MT map depicts the specific percentage loss of magnetization caused by a Gaussian RF pulse (4 ms duration, 220° nominal flip angle) applied 2 kHz off-resonance prior to nonselective excitation. This differs from the commonly used MT ratio (MTR, percentage reduction in steady state signal) by explicitly accounting for spatially varying T_1 relaxation times and flip angles (10) and results in higher contrast in the brain than the MT ratio (22). Additional minor corrections for flip angle inhomogeneity in the MT maps were applied as described by Weiskopf et al. (14).

Linear Relaxometry Model

Under the conditions of fast exchange, the cross-relaxation time between different water components is assumed to be much shorter than the MR relaxation times. In this case, the measured longitudinal relaxation rate is a weighted sum of the relaxation rates of the various contributory components (7):

$$R_1 = \sum_i f_i R_{1i} \tag{1}$$

where f_i is the fraction of spins in pool i with relaxation rate R_{1i}. In the absence of any exogenous contrast agents, the measured R_1 will predominantly depend on the fraction of free water spins, as well as the fraction of bound water spins at macromolecular sites and, on a smaller contribution, from iron sites (8,23). In this case, equation 1 becomes:

$$R_1 = R_{1f} + f_M r_{1M} + f_{FE} r_{1FE} + \sum_j f_j R_{1j} \tag{2}$$

where R_{1f} is the relaxation rate of free water; f_M is the fraction of spins bound to macromolecules; r_{1M} is the relaxivity at macromolecular sites (ie, $R_{1M} - R_{1f}$) where

Table 1
Summary Statistics for the Global Parameters of the Linear Model Across the Cohort at a Threshold of 50%

Parameter	Mean	Standard Deviation	Coefficient of Variation
β_0 (s^{-1})	0.2677	0.0142	5.32%
β_1 (s^{-1}/p.u.)	0.3971	0.0184	4.64%
β_2	0.0025	0.0009	37.15%

R_{1M} is the relaxation rate at macromolecular sites, f_{FE} is the fraction of spins at iron sites, and r_{1FE} is the relaxivity at iron sites; the index j sums over all potential unspecified contributions that remain.

Estimating Model Parameters

A model of R_1 based purely on imaging data can be constructed from Eq. 2 by replacing the known contributors to R_1 with surrogate markers. Using the MT and R_2^* maps from the MPM protocol as surrogate markers for the macromolecular and iron concentrations, respectively, the model can be expressed as a function of spatial position, r, as:

$$R_1(r) = \beta_0 + \beta_1 MT(r) + \beta_2 R_2^*(r) + \varepsilon(r) \qquad [3]$$

Here the set of β parameters are global constants and $\varepsilon(r)$ is the spatially specific residual encompassing the unspecified contributions to R_1 and noise. For a given subject, a model matrix, $\mathbf{M}$, is constructed with three columns: unity, MT, and R_2^* (Fig. 1). In this case, the β parameters are the model coefficients and least squares solution to the matrix equation $R_1 = \mathbf{M}\beta$, and the residuals are the difference between the measured and synthetic R_1 values (ie, $\varepsilon = R_1 - \mathbf{M}\beta$).

The parameters of the linear relaxometry model were estimated for each volunteer separately by fitting the relationship across all brain voxels (excluding cerebrospinal fluid, which does not contain appreciable amounts of macromolecules or iron and is not well-characterized by the particular acquisition protocol used in this study). Brain voxels were identified by automated segmentation using SPM8 (24). All voxels with a gray or white matter probability >50% and a cerebrospinal fluid probability <50% were pooled to estimate the global, tissue-independent β parameters as well as a spatial map of the residual error on a subject-by-subject basis. The accuracy of the model was assessed by calculating a synthetic R_1 map from the β parameters (ie, $\mathbf{M}\beta$). The Pearson coefficient between the synthetic and measured R_1 values was calculated for each subject.

RESULTS

A single subject example data set is shown in Fig. 2 along with the model estimated R_1 and the residuals (ie, the difference between the estimated and measured R_1 values). The linear model fitted well with a mean Pearson coefficient across the entire cohort of 0.93 ± 0.03. The resulting β parameters are summarized for the group

FIG. 2. Exemplary single subject data from the cohort using a masking threshold of 30% on the tissue probabilities. The global β coefficients for this subject were: 0.2692 s^{-1}, 0.3979 s^{-1}/p.u., and 0.0011. The Pearson coefficient of the model in this subject was 0.96. (**a**) Measured R_1 map. (**b**) R_1 map synthesized using the model coefficients. (**c**) Spatial map of the model residuals (ie, the difference between the measured and synthesized R_1 maps). (**d**) Synthesized R_1 values plotted against the measured R_1 values across the whole brain illustrates the high correspondence between the two R_1 measures.
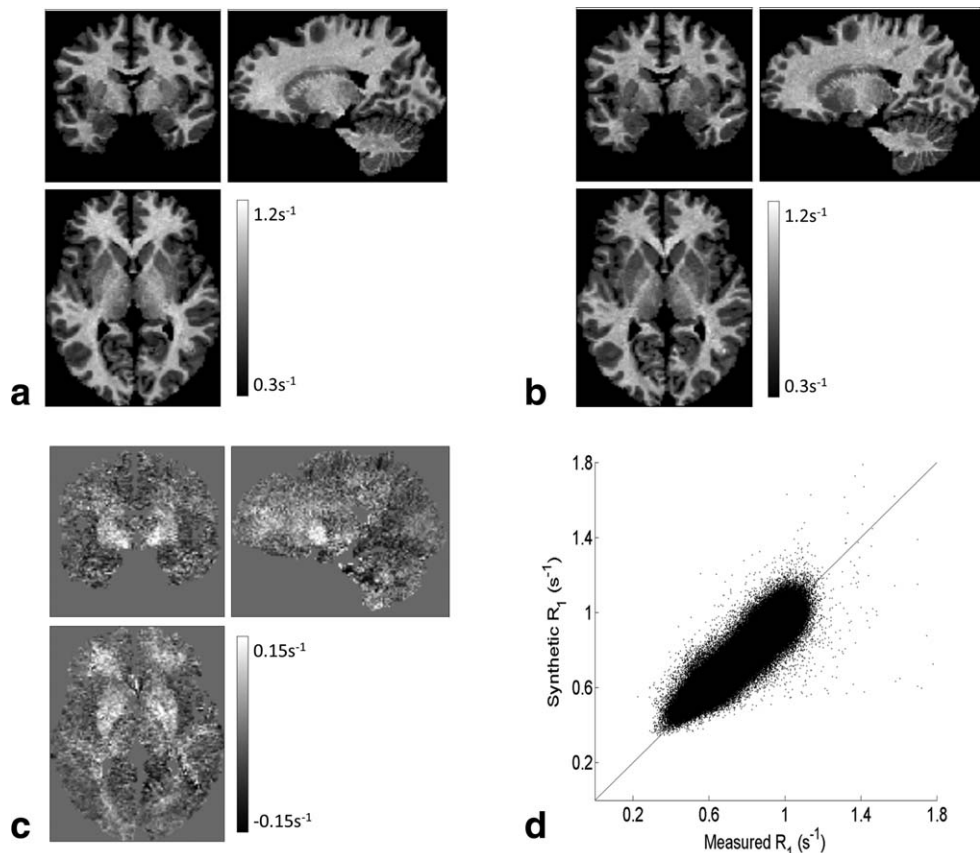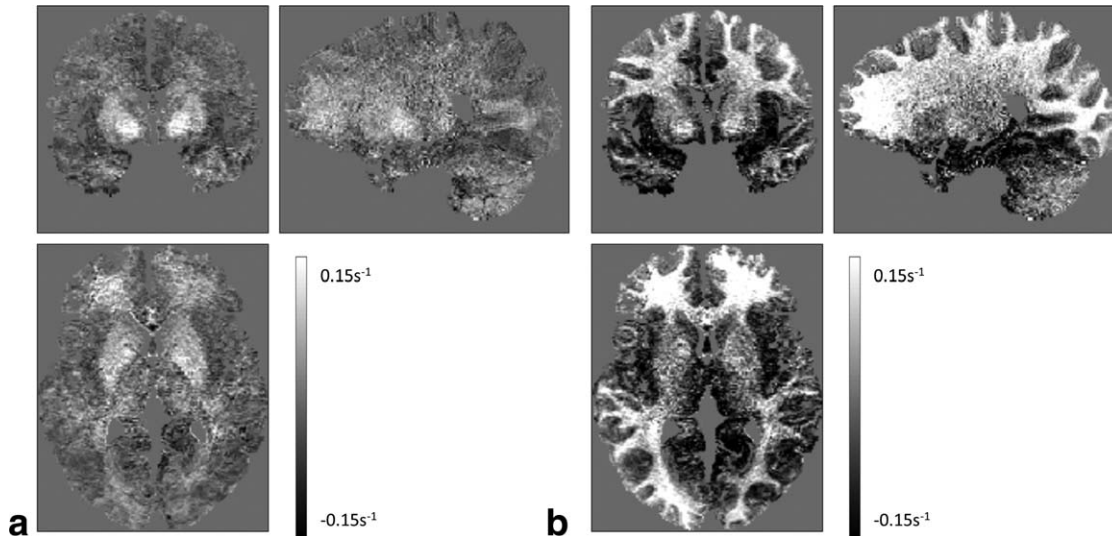
FIG. 3. Residuals from the linear model were significantly lower and contained far fewer anatomical structure and bias field effects when MT (**a**) rather than MTR (**b**) was used as a surrogate for macromolecules.

in Table 1. The coefficient of variation across volunteers was <5.5% for both β_0 and β_1 but rises to 37.2% for β_2.

The residuals were generally close to or within the acquisition noise level (14). Within the whole brain, they are centered at $-0.13 \pm 0.34\%$ across the cohort. Examining the residuals by tissue class revealed a bias of 1.62 $\pm$ 0.38% toward lower model R_1 values in white matter and a bias of 0.97 $\pm$ 0.52% toward higher model R_1 values in gray matter. The residual maps show that the greatest deviation of the model to the measured R_1 occurred within the basal ganglia, where it was underestimated by the model to varying degrees but in the order of 10%.

The β_0 parameter corresponded directly to the relaxation rate of free water. The estimated longitudinal relaxation time (T_1) of free water in brain tissue was 3.736 ± 0.198s.

DISCUSSION

A single set of β parameters sufficed to model R_1 across the whole brain, incorporating voxels from both gray and white matter. The model parameters describing the influence of free water and MT on R_1 were highly stable across this large cohort, suggesting that underlying microstructural differences due to macromolecular content are well captured by the MT map across both gray and white matter. This may be due to the fact that the transfer times are similar in gray and white matter (25). In agreement with the well-established two-site-fast-exchange model (2,7,23,26), the contribution from macromolecular components has been shown to be the dominant factor within the model. In addition, it has been shown that when gray and white matter are considered concurrently water content is a better predictor of R_1 variation than is iron content (8). The β_0 parameter appears to give a reliable estimate of the longitudinal relaxation rate of free water (R_{1f}) that is in keeping with values reported in the literature [see Table 1 in Rooney et al. (23)]. The remaining components of the model contain

inseparable components: the fraction of the spins at the site and the relaxivity of the site. For example, the β_1MT term of the model corresponds to the product of the macromolecular bound water fraction and the relaxivity at these macromolecular sites. Either of these components may change depending on the local microstructure. To separate the contributions and validate this model further, one or the other factor must be known. The bound water fraction can be measured histologically using calorimetric approaches, as has been done for white matter (3). Using the histological estimate of water fraction and combining it with our results yields a relaxivity estimate of 3.687 ± 0.198s^{-1} for WM, which is in good agreement with the literature (23).

Post mortem validation has shown high correspondence between R_2^* and iron content (13) and between MTR and myelin content (12). The fact that the β parameters largely showed good stability across this large cohort (age range, 19–75 y) validates our use of MT and R_2^* as surrogate markers for macromolecular and iron content. When the MTR measure was used in the model, the model coefficients were less stable and the model residuals were increased with anatomical and bias field structure present (Fig. 3). The stability of the model coefficients also suggests that they could be used to generate an estimated R_1 map directly from MT and R_2^* maps. Applying the model in such a way would facilitate a reduction in the total scan time for the quantitative MPM approach. It would also allow a synthetic quantitative map to still be calculated from suboptimal data (eg, if motion occurred during part of the protocol). The volunteers included in this analysis were all healthy volunteers with no evidence of cognitive impairment. Because we did not study patients, we cannot conclude whether a different set of model parameters may be required in pathological conditions. If they were, then the resulting parameters may become a diagnostic measure.

The model parameter describing the R_1 dependence on R_2^* (ie, β_2) had a markedly higher coefficient of variation
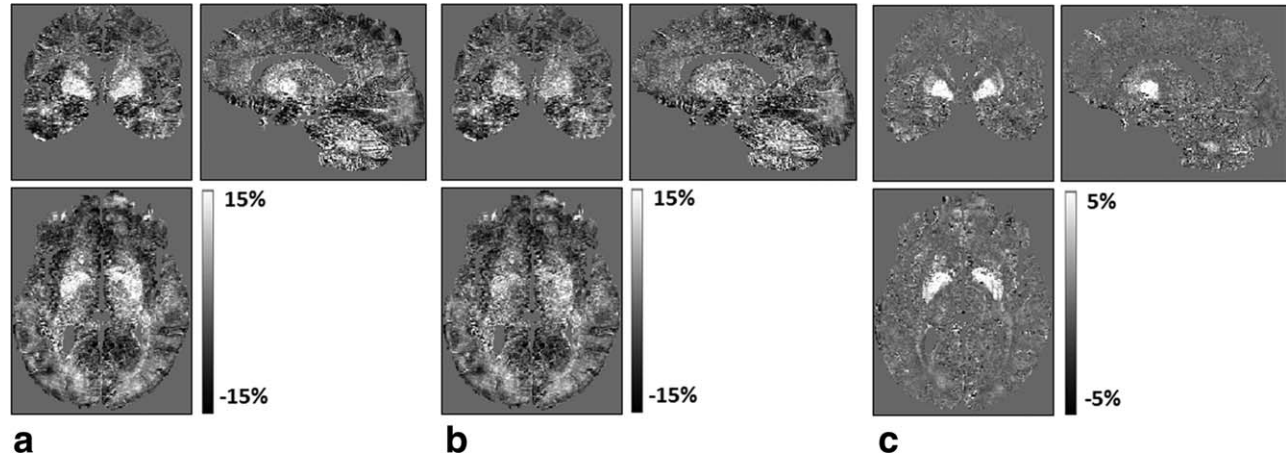
FIG. 4. Normalized residuals expressed in percent units from the linear model incorporating free water and macromolecular content (**a**) were reduced by also including an iron term (**b**). (**c**) The difference highlights iron-rich structures, such as the pallidum and dentate nucleus, in which the residuals were particularly reduced.

across volunteers than the free water or macromolecular terms. For the majority of the brain, the model performs well without the inclusion of the iron term, and the Pearson coefficient remains high (mean, 0.92). However, inclusion of the iron term via the R_2^* measure reduces the residuals for high iron structures, such as the basal ganglia and dentate nucleus (Fig. 4). This is to be expected, since it is in these structures that iron will contribute most significantly to R_1. Nonetheless, the residuals remain highest in these structures, suggesting that the iron effects are not described fully by the model. Additional or higher-order terms (eg, accounting for the different chemical forms in which iron is present in vivo (27)), may be required to more fully model the true R_1 variation in these structures. Additionally, the comparatively smaller contribution from iron sites may be poorly estimated because of the higher noise level in the R_2^* map estimated by our MPM protocol which uses a maximal echo time of 19.70 ms and because the multiecho three-dimensional FLASH volumes used to calculate the MT and R_1 maps are averaged resulting in an effective echo time of 8.45 ms and therefore residual R_2^* weighting. It has also been suggested that the measured R_2^* will depend on the orientation of white matter fibers with respect to the main field (28–30). These effects are currently not accounted for, though it may be possible to extend the model to include them.

The residuals of the model fit can have a variety of sources, typically falling into two categories: unknown or unspecified model terms, as discussed above, and noise. In some cases, the residuals are high because they capture a spatially coherent form of noise (ie, artifact) present in one or more of the maps used in the model. This is most typically caused by subject motion during the acquisition of one of the constituent three-dimensional FLASH volumes of the MPM protocol. Because the volumes combine in different ways to calculate each of the quantitative maps such motion can lead to inconsistencies across the model matrix components, which may in turn be captured by the residuals. This feature raises the interesting possibility of using the general linear relaxometry model

for artifact characterization and correction. Many opportunities arise from the application of this model such as further understanding R_1 dependencies, potential disease biomarkers, and artifact correction.

CONCLUSIONS

We have shown that a general linear model of longitudinal relaxation can be applied voxel-wise across the whole brain by using MT and effective transverse relaxation maps as surrogate concentrations for macromolecules and iron, respectively. This model fits well and provides a single set of model parameters per individual that is remarkably stable across the cohort.

ACKNOWLEDGMENTS

REFERENCES

1. Fatouros PP, Marmarou A. Use of magnetic resonance imaging for in vivo measurements of water content in human brain: method and normal values. J Neurosurg 1999;90:109–115.
2. Fatouros PP, Marmarou A, Kraft KA, Inao S, Schwarz FP. In vivo brain water determination by T1 measurements: effect of total water content, hydration fraction, and field strength. Magn Reson Med 1991;17:402–413.
3. Kaneoke Y, Furuse M, Inao S, Saso K, Yoshida K, Motegi Y, Mizuno M, Izawa A. Spin-lattice relaxation times of bound water—its determination and implications for tissue discrimination. Magn Reson Imaging 1987;5:415–420.
4. Shuter B, Wang SC, Roche J, Briggs G, Pope JM. Relaxivity of Gd-EOB-DTPA in the normal and biliary obstructed guinea pig. J Magn Reson Imaging 1998;8:853–861.
5. Donahue KM, Burstein D, Manning WJ, Gray ML. Studies of Gd-DTPA relaxivity and proton exchange rates in tissue. Magn Reson Med 1994;32:66–76.
6. Kamman RL, Go KG, Brouwer W, Berendsen HJ. Nuclear magnetic resonance relaxation in experimental brain edema: effects of water

concentration, protein concentration, and temperature. Magn Reson Med 1988;6:265–274.

7. Fullerton GD, Potter JL, Dornbluth NC. NMR relaxation of protons in tissues and other macromolecular water solutions. Magn Reson Imaging 1982;1:209–226.

8. Gelman N, Ewing JR, Gorell JM, Spickler EM, Solomon EG. Interregional variation of longitudinal relaxation rates in human brain at 3.0 T: relation to estimated iron and water contents. Magn Reson Med 2001;45:71–79.

9. Wolff SD, Balaban RS. Magnetization transfer contrast (MTC) and tissue water proton relaxation in vivo. Magn Reson Med 1989;10:135–144.

10. Helms G, Dathe H, Kallenberg K, Dechent P. High-resolution maps of magnetization transfer with inherent correction for RF inhomogeneity and T1 relaxation obtained from 3D FLASH MRI. Magn Reson Med 2008;60:1396–1407.

11. Helms G, Piringer A. Simultaneous measurement of saturation and relaxation in human brain by repetitive magnetization transfer pulses. NMR Biomed 2005;18:44–50.

12. Schmierer K, Scaravilli F, Altmann DR, Barker GJ, Miller DH. Magnetization transfer ratio and myelin in postmortem multiple sclerosis brain. Ann Neurol 2004;56:407–415.

13. Langkammer C, Krebs N, Goessler W, Scheurer E, Ebner F, Yen K, Fazekas F, Ropele S. Quantitative MR imaging of brain iron: a postmortem validation study. Radiology 2010;257:455–462.

14. Weiskopf N, Suckling J, Williams G, Correia MM, Inkster B, Tait R, Ooi C, Bullmore ET, Lutti A. Quantitative multi-parameter mapping of R1, PD*, MT, and R2* at 3T: a multi-center validation. Front Neurosci 2013;7:1–11.

15. Helms G, Dechent P. Increased SNR and reduced distortions by averaging multiple gradient echo signals in 3D FLASH imaging of the human brain at 3T. J Magn Reson Imaging 2009;29:198–204.

16. Helms G, Dathe H, Dechent P. Quantitative FLASH MRI at 3T using a rational approximation of the Ernst equation. Magn Reson Med 2008;59:667–672.

17. Lutti A, Stadler J, Josephs O, Windischberger C, Speck O, Bernarding J, Hutton C, Weiskopf N. Robust and fast whole brain mapping of the RF transmit field B1 at 7T. PLoS One 2012;7:e32379.

18. Preibisch C, Deichmann R. Influence of RF spoiling on the stability and accuracy of T1 mapping based on spoiled FLASH with varying flip angles. Magn Reson Med 2009;61:125–135.

19. Sereno MI, Lutti A, Weiskopf N, Dick F. Mapping the Human Cortical Surface by Combining Quantitative T1 with Retinotopy. Cereb Cortex 2013;23:2261–2268.

20. Dick F, Tierney AT, Lutti A, Josephs O, Sereno MI, Weiskopf N. In vivo functional and myeloarchitectonic mapping of human primary auditory areas. J Neurosci 2012;32:16095–16105.

21. Lutti A, Dick F, Sereno MI, Weiskopf N. Using high-resolution quantitative mapping of R1 as an index of cortical myelination. Neuroimage 2013:1–13.

22. Helms G, Dathe H, Dechent P. Modeling the influence of TR and excitation flip angle on the magnetization transfer ratio (MTR) in human brain obtained from 3D spoiled gradient echo MRI. Magn Reson Med 2010;64:177–185.

23. Rooney WD, Johnson G, Li X, Cohen ER, Kim S-G, Ugurbil K, Springer CS. Magnetic field and tissue dependencies of human brain longitudinal 1H2O relaxation in vivo. Magn Reson Med 2007;57:308–318.

24. Ashburner J, Friston KJ. Unified segmentation. Neuroimage 2005;26:839–851.

25. Helms G, Hagberg GE. Pulsed saturation of the standard two-pool model for magnetization transfer. Part I: the steady state. Concepts Magn Reson 2004;21A:37–49.

26. Li X, Rooney WD, Springer CS. A unified magnetic resonance imaging pharmacokinetic theory: intravascular and extracellular contrast reagents. Magn Reson Med 2005;54:1351–1359.

27. Connor JR, Menzies SL. Relationship of iron to oligodendrocytes and myelination. Glia 1996;17:83–93.

28. Bender B, Klose U. The in vivo influence of white matter fiber orientation towards B(0) on T2* in the human brain. NMR Biomed 2010;23:1071–1076.

29. Wharton S, Bowtell R. Fiber orientation-dependent white matter contrast in gradient echo MRI. Proc Natl Acad Sci U S A 2012;109:18559–18564.

30. Wharton S, Bowtell R. Gradient echo based fiber orientation mapping using r2* and frequency difference measurements. Neuroimage 2013;83:1011–1023.